Available online at www.sciencedirect.com

ScienceDirect

Procedia Structural Integrity 28 (2020) 1116–1124

Structural Integrity Procedia

www.elsevier.com/locate/procedia

1st Virtual European Conference on Fracture

Bonded structures improvement by the dual adhesive technique

C.L. Ferreira[a], R.D.S.G. Campilho[a,b]*, R.D.F. Moreira[a,b]

[a]*Departamento de Engenharia Mecânica, Instituto Superior de Engenharia do Porto, Instituto Politécnico do Porto, Rua Dr. António Bernardino de Almeida, 431, 4200-072 Porto, Portugal.*

[b]*INEGI – Pólo FEUP, Rua Dr. Roberto Frias, s/n, 4200-465 Porto, Portugal.*

Abstract

A common technique to reduce stress gradients in adhesive joints is to use the dual adhesive technique, which has proven to reduce peak stresses in single-lap joints. However, other joint configurations could benefit from this technique. This work experimentally and numerically evaluates stepped-lap dual-adhesive joints (DAJ) between aluminum adherends, for various overlap lengths (L_O), and carries out a detailed comparison with stepped-lap single-adhesive joints (SAJ) with the same individual adhesives (Araldite® AV138 and Araldite® 2015). The joint behavior was predicted by cohesive zone modelling (CZM) with a triangular law. The analysis of the results is presented in the form of failure modes, stress analysis, maximum load (P_m) and energy required to failure (U). It was concluded that, in general, CZM presented precise predictions and are a valuable tool for the design of both SAJ and DAJ. However, no significant increase in strength was achieved with DAJ, although using more ductile adhesive can promote better DAJ results.

Keywords: Adhesive joints; Stepped-lap joints; Cohesive zone models; Dual adhesive joints.

1. Introduction

Adhesive bonding has been used in fields as diverse as aerospace (Désagulier 2011) and aeronautics (Hart-Smith 2011), defence, automotive (Burchardt 2011), electronics (Jung and Kim 2011), construction (Hartung and Boehm 2011), footwear (Martín-Martínez 2011), wood industry, marine (Davies 2011), railway (Suzuki 2011) and others.

* Corresponding author. Tel.: +351 939526892; fax: +351 228321159.
E-mail address: raulcampilho@gmail.com (R.D.S.G. Campilho).

2452-3216
10.1016/j.prostr.2020.11.126

The use of adhesive joints in industrial applications has increased in recent years, to the detriment of traditional bonding methods such as welding, brazing, bolting and riveting (Petrie 2000). Actually, adhesive joints promote an improved load distribution on a larger surface than mechanical joints, which leads to lower stress concentrations in the adherend materials, are less prone to corrosion and fatigue problems, which are characteristic of traditional joints, and are fluid sealant (Petrie 2000). However, they do have some disadvantages, such as the requirement of surface treatment, possible need of temperature and pressure for curing, performance depending on the processing conditions, limited durability under extreme service conditions (especially temperature), poor resistance to peeling, difficult quality control and lack of unified procedure for design (Petrie 2000). The most commonly used adhesive joint configuration is the single-lap joint, due to the simplicity associated with its manufacture (da Silva et al. 2011). However, single-lap joints promote excessive rotation of the adherends due to the non-collinearity of the applied load, which causes considerable peel stresses. In addition, high shear stress gradients are observed due to the differential deformation effect of the adherends (Campilho et al. 2009). Other types of joints are available that reduce the stress variation along the adhesive, such as stepped-lap joints. The main advantages of these joints compared to single-lap joints are the reduction of peel and shear peak stresses and the better aesthetics (Silva et al. 2018). The biggest disadvantage is the difficulty and time spent in machining the adherends, which leads to a more expensive fabrication overall. It is possible to minimize these stress gradients with mixed-adhesive joints, whose bondline is composed of two adhesives, one more flexible at the ends and another stiffer at the interior (da Silva and Adams 2007). This type of joints can also be seen as a solution to joints that need to withstand high and low temperatures present in aeronautical applications (da Silva et al. 2007). The use of a high modulus brittle adhesive at the interior of the joint maintains good resistance to high temperatures while, at low temperatures, the presence of a ductile adhesive at the ends of the joint avoids the appearance of stress concentrations which would cause premature failure (da Silva et al. 2007). The mixed adhesive technique is well studied in single-lap joints (Breto et al. 2017). However, other geometries, such as stepped-lap adhesive joints, could also benefit from this combination of adhesives to reduce stress variations along the adhesive joint. The existence of reliable modelling techniques is fundamental to study and perform geometrical optimization to adhesive joints. CZM combined with FEM damage modelling is an technique that uses fracture mechanics approach with cohesive elements to simulate crack growth along specified planes and traditional FEM modelling in the regions where the damage was considered (Carvalho and Campilho 2016). CZM uses one or more interfaces/regions of fracture, which can be artificially introduced into structures, thus enabling damage growth by employing traction-separation laws for modelling solid regions or interfaces. Traction-separation laws are commonly established through linear relations in each of the loading steps. However, one or more steps may be defined differently, to more accurately represent the behavior of other materials.

The mixed adhesive technique has been widely addressed in the past for single-lap joints, by either experimentation and/or FEM modelling (da Silva and Lopes 2009, Akpinar et al. 2013, Bavi et al. 2013). Öz and Özer (2017) carried out an experimental investigation on the failure loads of mono and bi-adhesive joints. The study initiated by comparing the failure loads of single-lap joints of mono adhesive bonded with the AV138, 2015 and 3M DP-8005, showing that the 2015 provides the best results. Secondly, mixed adhesive joints were studied with the following adhesive combinations: AV138 (middle overlap) + 2015 (overlap ends) and AV138 (middle overlap) + DP-8005 (overlap ends). It was concluded that the bi-adhesive joints provide a higher joint strength than the joints with only one adhesive even if the ductile adhesive has a higher joint strength than the stiff adhesive. Jairaja and Naik (2019) experimentally and numerically investigated the strength of single-lap joints between dissimilar adherends, and either with the single-adhesive joint (SAJ) or double-adhesive joint (DAJ) configurations. In this investigation, single-lap joints were used with the AV138 and 2015 in CFRP and aluminum adherends. In the mixed adhesives joints, the 2015 was used at the overlap ends and the AV138 in the middle. To monitor the relative displacements between the adherends, Digital Image Correlation (DIC) was employed. On the other hand, peel and shear stresses were assessed by the FEM using Abaqus®. For the SAJ, the 2015 resulted in higher joint strengths compared to the AV138. The DAJ revealed a substantial performance improvement over the SAJ, especially for a small proportion of brittle adhesive at the overlap center (20%). The displacement, strain and stress contours obtained from DIC and FEM were compared and showed a good match, revealing the effect of the DAJ technique on the load distribution at the overlap.

This work experimentally and numerically evaluates stepped-lap DAJ between aluminum adherends, for various L_O, and carries out a detailed comparison with stepped-lap SAJ with the same individual adhesives (Araldite®

AV138 and Araldite® 2015). The joint behavior was predicted by CZM with a triangular law. The analysis of the results is presented in the form of failure modes, stress analysis, P_m and U.

2. Experimental work

2.1. Adherend and adhesive properties

The adherend material chosen for the joints was the AW6082 T651 high strength aluminum alloy which, according to the supplier's data, has a tensile strength of approximately 340 MPa. For input in the numerical models, this material was tested in bulk tension using dogbone specimens according to the standard ASTM-E8M-04 (2004). The stress-strain (σ-ε) curves of this material were obtained as described in the standard. The following properties are relevant for the present work: Young's modulus (E) of 70.07±0.83 GPa, tensile yield stress (σ_e) of 261.67±7.65 MPa, tensile strength (σ_f) of 324±0.16 MPa and tensile failure strain (ε_f) of 21.70±4.24% (Campilho et al. 2011). Two adhesives were evaluated: Araldite® AV138 (brittle epoxy) and Araldite® 2015 (ductile epoxy). The tensile mechanical properties (E, σ_e, σ_f and ε_f) were found by bulk dogbone specimens, fabricated as specified in the Standard NF T 76-142. The shear mechanical properties were estimated by Thick Adherend Shear Tests (TAST). The shear modulus (G) in particular was estimated by the Hooke's law from the knowledge of E and Poisson's coefficient (ν). It should also be mentioned that σ_e and the shear yield stress (τ_e) were calculated for a plastic strain of 0.2% in the respective curves. The tensile toughness (G_{IC}) and shear toughness (G_{IIC}) were obtained from Double-Cantilever Beam (DCB) and End-Notched Flexure (ENF) tests, respectively, after test data analysis by suitable data reduction techniques. The detailed fabrication and testing procedures for these specimens are described in a previous work (Leitão et al. 2016). The obtained properties for the two adhesives are presented in Table 1.

Table 1 – Mechanical and fracture properties of the adhesives AV138 and 2015 (Campilho et al. 2011, Campilho et al. 2013).

Property	AV138	2015
Young's modulus, E [GPa]	4.89±0.81	1.85±0.21
Poisson's ratio, ν	0.35 [a]	0.33 [a]
Tensile yield stress, σ_e [MPa]	36.49±2.47	12.63±0.61
Tensile strength, σ_f [MPa]	39.45±3.18	21.63±1.61
Tensile failure strain, ε_f [%]	1.21±0.10	4.77±0.15
Shear modulus, G [GPa]	1.81 [b]	0.70 [b]
Shear yield stress, τ_e [MPa]	25.1±0.33	14.6±1.3
Shear strength, τ_f [MPa]	30.2±0.40	17.9±1.8
Shear failure strain, γ_f [%]	7.8±0.7	43.9±3.4
Toughness in tension, G_{IC} [N/mm]	0.20 [c]	0.43±0.02
Toughness in shear, G_{IIC} [N/mm]	0.38 [c]	4.70±0.34

[a] manufacturer's data

[b] estimated from the Hooke's law using E and ν

[c] estimated in Campilho et al. (2011)

2.2. Experimental details

Fig. 1 depicts the stepped-lap joint geometry and relevant parameters. The main geometrical parameters considered in this work are: L_O=12.5, 25, 37.5 and 50 mm, adherends' thickness t_P=3 mm, adhesive thickness t_A=0.2 mm, step transitions' adhesive thickness t_{A1}=0.2 mm, width B=25 mm and joint total length L_T=180 mm. Apart from the three SAJ configurations, a DAJ configuration was evaluated: 2015/AV138/2015 (i.e., 2015 to bond the outer steps and AV138 to bond the middle step).

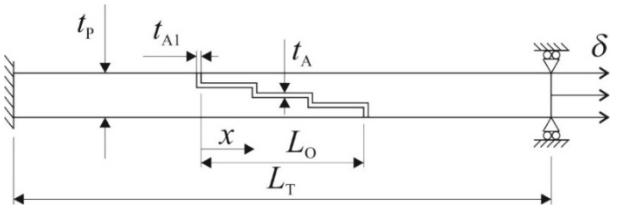

Fig. 1 – Stepped-lap joints' geometry and relevant dimensions.

For each joint configuration (either SAJ or DAJ), four specimens were manufactured and tested. The initial stage of joint fabrication was the cutting of the supplied plate to the adherends' specified B and length. The next stage was the execution of the steps, which was accomplished by milling operations, performed in a High-Speed Steel (HSS) mill. The surface oxide layer and contaminants were removed by sand blasting with corundum sand and cleaned with acetone, respectively. To ensure longitudinal alignment and assure the specified t_A throughout the adhesive layer, a steel jig was used for joint assembly. For the DAJ, during the adhesives' pouring stage, and in order to minimize inter-mixing of both adhesives, a thin Teflon® barrier was placed at the end of each step. The cure of the adhesive was performed at room temperature for at least 48h hours, and pressure was applied to the specimens during this period. The excess of adhesive at the overlap edges was removed by milling. The mechanical tests were performed at room temperature in a Shimadzu AG-X 100 machine, equipped with a 100 kN load cell and with a testing speed of 1 mm/min. For each joint type, a minimum of three valid results was always attained.

3. Numerical work

3.1. Construction of the numerical models

The numerical work was performed in Abaqus® considering a two-dimension analysis and plane-strain conditions, with a non-linear geometrical formulation (Pandey and Narasimhan 2001). Elastic-plastic isotropic solid elements were considered for the adherends. In the case of the adhesive layer, it was modelled either with CZM elements, to enable crack growth modelling, or as elastic solid elements, to obtain the stress distributions at the adhesive mid-thickness. Four-node quadrilateral solid elements (CPE4) and four-node cohesive elements (COH2D4) were employed in the models. In the CZM models, a single row of cohesive elements with square shape was implemented along the adhesive layer. The adhesive layer was modelled with a specified number of horizontal and vertical segments with material Fig. 2 shows a mesh example used for the failure analysis with CZM elements for L_O=25 mm.

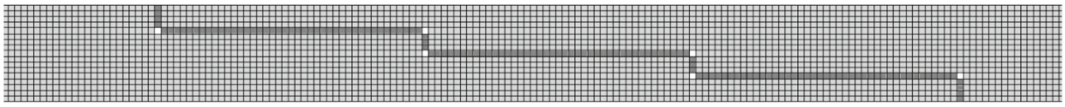

Fig. 2 – Mesh example at the overlap for L_O=25 mm.

The mesh used to obtain the stress distributions is significantly more refined to promote accuracy in the stress plots. Therefore, ten solid elements were considered throughout the adhesive layer thickness. The boundary conditions applied to the models consisted of clamping one of the joint edges, while the other edge was subjected to a tensile displacement concurrently with transverse restraining.

3.2. CZM theory

Relationships among stresses and relative displacements linking similar nodes of cohesive elements are the fundament of the CZM. Additionally, those relations (often entitled CZM laws) may be established in pure and

mixed mode, and make possible to capture the material's behavior up to failure (Luo et al. 2016). This study relies on triangular pure and mixed-mode laws to model the adhesive layer. Under pure-mode loading, damage initiation occurs when the cohesive strength in tension or shear (t_n^0 or t_s^0, respectively) is attained, i.e., the material's elastic behavior is cancelled and degradation starts (Sane et al. 2018). Furthermore, the crack propagates up to the adjacent pair of nodes when the values of current tensile or shear cohesive stresses (t_n or t_s, respectively) become nil. Under mixed-mode loading, stress and/or energetic criteria are often used to combine the pure-mode laws, and damage begins when the mixed mode cohesive strength (t_m^0) is reached (Dimitri et al. 2015). This study focused on the quadratic nominal stress criterion and a linear power law form for the damage initiation and growth, respectively. This model is described in detail in the work of Rocha and Campilho (2018). The adhesives' properties used in Abaqus® are depicted in Table 1, considering t_n^0 and t_s^0 as the values of σ_f and shear strength (τ_f).

4. Results

4.1. Failure modes

Cohesive failures were experimentally achieved for all bonded joints, thus denoting an efficient bonding between the adherends and adhesive. Experimentally, it was not possible to obtain full details of the failure paths. With the numerical models, it was possible to characterize the failure paths for each joint configuration and L_O. Table 2 presents a summary of the obtained failure paths and the adherends' maximum percentile plastic strain at P_m. The failure spots are defined as follows: outer step transitions (1), inner step transitions (2), outer steps (3) and middle step (4). Moreover, mention to P_m will be used for the description, which will be detailed only in Section 4.4.

Table 2 – Numerical failures for the different adhesive joint configurations.

		12.5	25	37.5	50
SAJ	Failure path	1-2-3-4	1-2-3-4	1-2-3-4	1-2-3-4
AV138	Plastic strain [%]	0.14	1.68	2.64	3.80
SAJ	Failure path	1-2-3-4	1-2-3-4	1-2-3-4	1-2-3-Plast.
2015	Plastic strain [%]	-	0.88	3.90	-
DAJ	Failure path	2-1-4-3	2-1-4-3	2-1-4-3	2-1-4-Plast
	Plastic strain [%]	-	1.61	12.58	-

First considering the SAJ, in the joints with the AV138, failure was identical irrespectively of L_O. Failure began at the outer step transitions (1), followed by inner step transitions (2). Damage then propagated to the outer steps (3), finishing in the middle step (4). The plastic strain progressively increased with L_O, corresponding to gradually higher P_m, up to 3.80% for L_O=50 mm. A similar scenario was found for the SAJ with the 2015. However, due to the higher P_m over the AV138, higher degree of plasticization was found and, inclusively, a tensile net failure of the adherends nearby (2) was found for L_O=50 mm. A significant variation of the failure sequence was registered for the DAJ, due to shifting the load transmission to the inner overlap. Thus, failure initiated at the inner step transitions (2), followed by the outer step transitions (1), the inner step (3), and finally either the outer steps (3) (up to L_O=37.5 mm) or adherend plasticization (L_O=50 mm). Due to the higher P_m involved, plastic strain was as high as 12.58% for L_O=37.5 mm.

4.2. Stress analysis

In the elastic analysis of joint stresses, peel (σ_y) and shear stress (τ_{xy}) distributions were considered, always normalized by the average shear stress (τ_{avg}) for the respective L_O. It was considered convenient to normalize L_O by using the variable x/L_O, where x represents the distance measured from the left edge of the adhesive layer. The stress plots relate to the mid-plane of adhesive, where the stresses are symmetrical. Only L_O=12.5 and 50 mm were considered. Fig. 3 and Fig. 4 represent σ_y/τ_{avg} and τ_{xy}/τ_{avg} stresses, respectively.

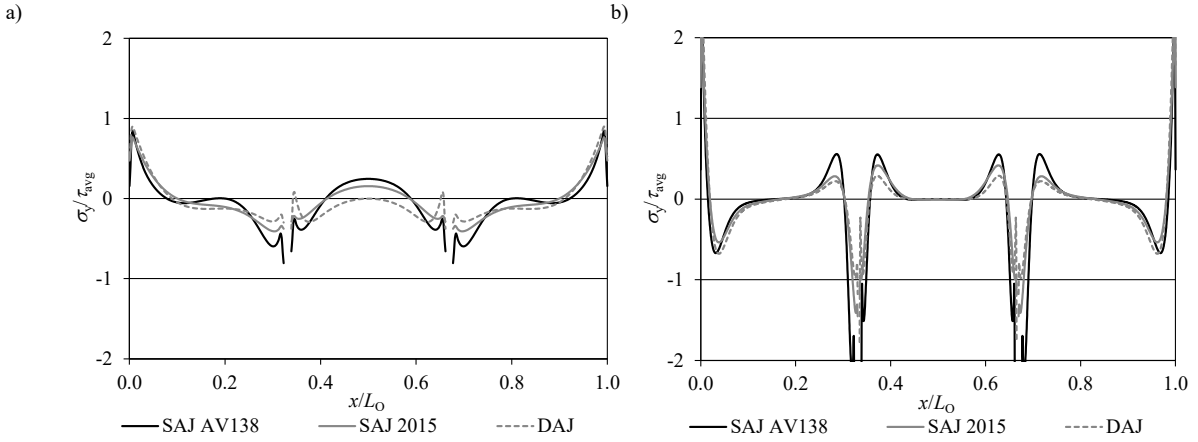

Fig. 3 – σ_y/τ_{avg} stresses for all joint configurations and L_O=12.5 (a) and 50 mm (b).

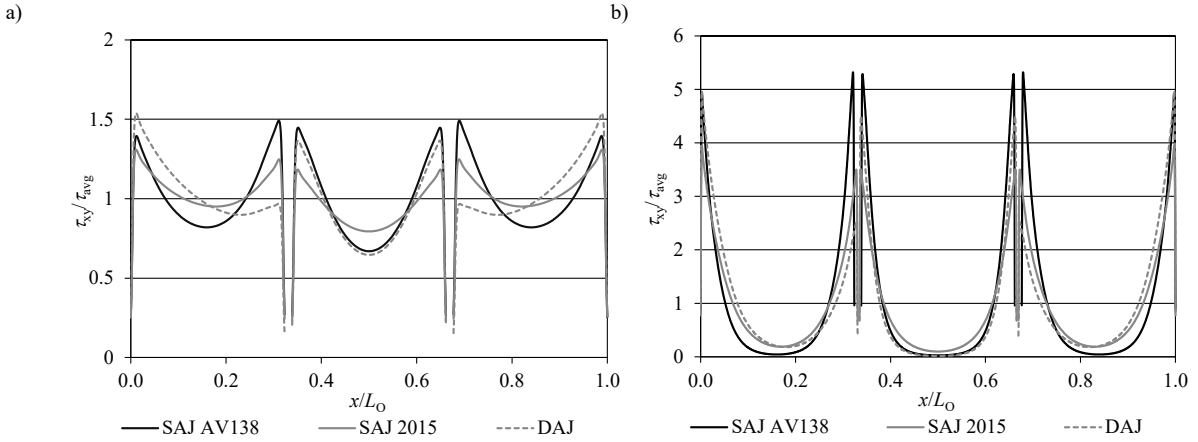

Fig. 4 – τ_{xy}/τ_{avg} stresses for all joint configurations and L_O=12.5 (a) and 50 mm (b).

It was concluded that, independently of L_O, σ_y stresses are generally much below τ_{avg}, except at the step edges. Apart from few joint configurations, σ_y stresses peak at the joint ends (x/L_O=0 and x/L_O=1), with smaller magnitude peaks at the step transitions ($x/L_O \approx 0.33$ and $x/L_O \approx 0.67$). Moreover, compressive σ_y stresses exist at the step transitions, while at the joint edges these are essentially peel peaks. The increase of L_O causes higher magnitude σ_y peak stresses in both tensile and compressive peaks. The choice of adhesive also has a major influence on the stress distributions. Actually, the reduction of the adhesive's stiffness tends to promote more uniform stress distributions, and this is clearly visible by comparing the two SAJ. For these joints, the highest σ_y/τ_{xy} peak stresses, always at x/L_O=0 and 1, were 0.85 for the AV138 and 0.76 for the 2015 (L_O=12.5 mm), and 2.96 for the AV138 and 2.34 for the 2015 (L_O=50 mm), thus diminishing with increasing the adhesives' compliance. By considering the DAJ, the use of a more compliant and ductile adhesive at the outer steps generally reduces σ_y stresses, but this effect is more noticeable at the inner overlap than at the overlap ends. Inclusively, potentially σ_y stresses become compressive at the inner step (for shorter L_O), which should result in an improved joint behavior. The maximum σ_y/τ_{avg} values were 0.90 (L_O=12.5 mm) and 2.95 (L_O=50 mm).

The analysis of τ_{xy} stresses showed that these slightly differ between the outer and inner steps. As with the conventional single-lap joint, τ_{xy} stresses are higher at the ends of the overlap and smaller at the inner overlap. This effect is also found in the stepped-lap joints, but to a much smaller extent due to cross-sectional reduction of the adherends at the overlap. Moreover, within each step, the stress curve resembles that of a single-lap joint. The

adhesive's stiffness also reflects on the maximum τ_{xy}/τ_{avg} peak stresses at x/L_O=0 and 1, except for the AV138, with advantage for less stiff adhesives: 1.49 for the AV138 and 1.31 for the 2015 (L_O=12.5 mm) and 5.32 for the AV138 and 3.95 for the 2015 (L_O=50 mm). Comparison between the SAJ and DAJ shows a noteworthy variation regarding the magnitude of τ_{xy} peak stresses, especially for short L_O. The general tendency consists of a major reduction of τ_{xy}/τ_{avg} stresses at the inner portion of the outer steps, a conflicting behavior at the overlap ends (either increasing or reducing τ_{xy}/τ_{avg} stresses, depending on the configuration), and an increase of peak stresses at the inner step's edges. The τ_{xy}/τ_{avg} peak stresses, although at different locations, were as follows: 1.54 (L_O=12.5 mm) and 4.97 (L_O=50 mm). Although the peak values cannot reveal a real difference, there is a clear tendency to shift the transmitted loads from the outer steps to the inner step.

4.3. Joint strength

Fig. 5 presents P_m as a function of L_O for the experimental and numerical results, being (a) SAJ and (b) DAJ. For the SAJ (Fig. 5 a), the highest P_m for L_O=12.5 mm was attained by the AV138, 19.3% higher than the 2015 (the percentile differences in this section are always calculated based on the experimental data). However, the joints' behavior clearly changes for higher L_O, since the AV138, due to its combined stiffness and brittleness, shows a reduced P_m increase with L_O, oppositely to the 2015. Thus, and according to the stress analysis performed in Section 4.2, the SAJ with the AV138 showed the highest peak stresses at the steps edges and at the transition between steps, because of the adhesive's stiffness. The brittle behavior of AV138 is then linked to sudden failure when these peak stresses surpass the adhesive's minor yielding capacity. Since the peak stresses largely increase with L_O, the increase of this geometric parameter does not translate into a major P_m benefit. In view of this, for L_O=25 mm the 2015 provides the highest P_m, surpassing the AV138 by 20.9%. L_O=50 mm confirms the worst results for the AV138, and best results for the 2015. The relative improvement of the 2015 is 48.4% over the AV138. Fig. 5 (b) presents the DAJ P_m results. The comparison between SAJ and DAJ shows that, for all considered L_O, the DAJ never provide a significant benefit. For L_O=12.5 mm, the best joint configuration is the SAJ with AV138 (P_m =6.25 kN), followed by the DAJ, with a relative difference of 15.68%. The DAJ becomes the best choice for L_O=25 mm, but only with a minor difference of 1.49% over the SAJ with 2015. For L_O=37.5 mm, the highest P_m occurred for the SAJ with 2015, but only surpassing the DAJ by 1.50%. The same joint behaved best for L_O=50 mm, although with a higher difference over the DAJ (11.47%).

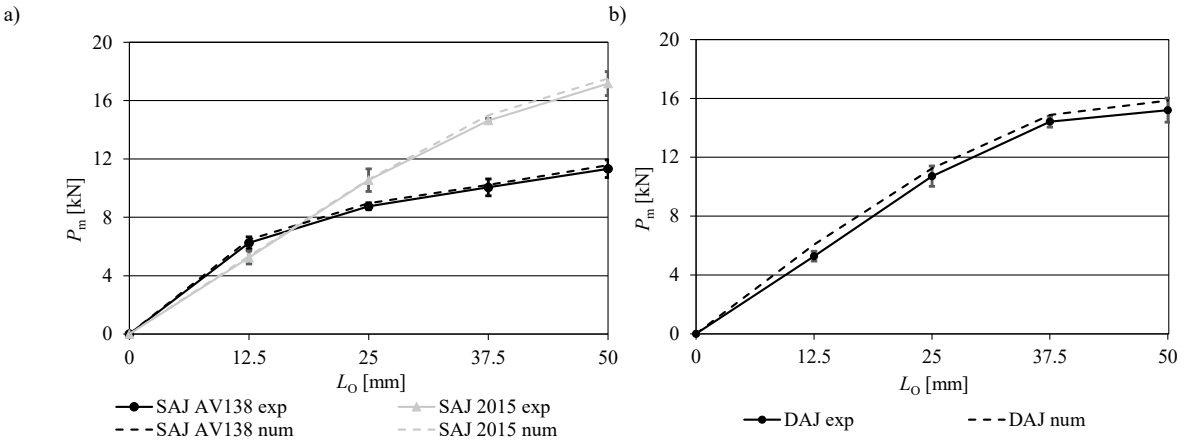

Fig. 5 – P_m-L_O plots for the SAJ (a) and DAJ (b).

The numerical P_m results showed a reasonable agreement comparing with the experiments. Considering the SAJ, a good agreement is visible for the AV138 and 2015 (highest deviations of 3.5 and 2.4%, respectively). For the DAJ, a small P_m over predicting trend is visible, with a maximum offset of 15.2% for L_O=12.5 mm, but much better predictions for the other L_O (differences below 5%).

4.4. Energy analysis

U at failure is a relevant parameter in the design of bonded joints, as it is linked to the required absorbed energy for a joint to cease to correctly perform its function. Thus, higher U corresponds to higher deformability of a joint within a structural before failure, more predictive failure and higher overall performance. Measurement of this parameter is accomplished by evaluating the area under the P-δ curve. In general, the experimental and numerical U measured from the respective P-δ curves were in close agreement and, thus, only the numerical values are discussed. Fig. 6 compares U for all L_O and both SAJ and DAJ.

Beginning the analysis by the SAJ, the AV138 resulted in the worst results, despite its strength, due to its brittleness, which makes the respective joints to fail under a marginal applied δ. The improved behavior of the 2015 is mainly related to the highest δ at failure of the joints bonded with this adhesive. To be noted that, for L_O=50 mm, the adherends of the SAJ with 2015 undergo significant plasticization (and tensile net failure), which makes U to largely increase from the L_O=37.5 mm condition. The DAJ typically gives results somehow close to the SAJ with 2015. Thus, from this analysis it becomes clear that no improvements can be found by the DAJ technique applied to stepped-lap joints, using the chosen adhesives. This behavior contrast with the common knowledge for single-lap joints and it is related to the uniformization of adhesive stresses promoted by the stepped geometry. However, a possible solution to improve the DAJ configuration would be to consider a set of two more ductile adhesives.

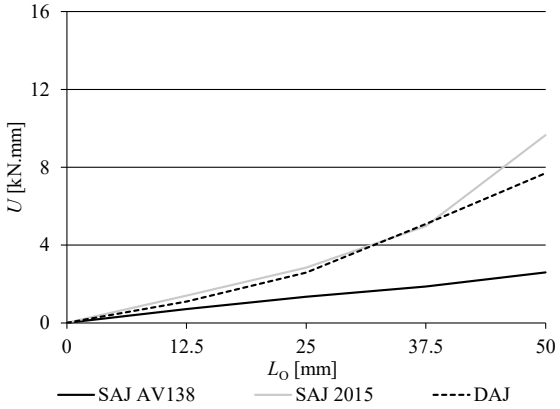

Fig. 6 – Numerical U-L_O plots for the SAJ and DAJ.

5. Conclusions

This work aimed at testing possible advantages in applying the DAJ technique, widely studied for single-lap joints, in stepped-lap joints. Furthermore, a CZM analysis enabled a detailed description of the joints' behavior. Initially, the experimental and especially numerical failures were addressed. Numerically, it was possible to capture the failure sequence and detect the amount of adherend plasticization. The stress analysis could not provide irrefutable evidence that the DAJ have a major advantage over SAJ, especially regarding σ_y, although the appearance of compressive peaks at the inner step is always positive. However, τ_{xy} stresses showed higher loads being transmitted by the inner step for the DAJ. The strength analysis revealed that, from this metrics, DAJ have no real benefit over SAJ. Actually, the 2015 was typically the best choice between the SAJ (except for the shortest L_O), and the DAJ only managed to provide better results using L_O=25 mm, giving a 1.49% difference. The CZM predictions were in general accurate. The U analysis equally showed no DAJ improvements over the SAJ condition, due to the uniformization of stresses compared to single-lap joints. However, it is considered that testing more ductile adhesives in the DAJ could provide an advantage in using this technique.

References

Akpinar, S., Aydin, M. D. and Özel, A., 2013. A study on 3-D stress distributions in the bi-adhesively bonded T-joints. Applied Mathematical Modelling 37(24), 10220-10230.

ASTM-E8M-04 (2004). Standard test methods for tension testing of metallic materials [Metric]. West Conshohocken, PA, ASTM International.

Bavi, O., Bavi, N. and Shishesaz, M., 2013. Geometrical Optimization of the Overlap in Mixed Adhesive Lap Joints. The Journal of Adhesion 89(12), 948-972.

Breto, R., Chiminelli, A., Lizaranzu, M. and Rodríguez, R., 2017. Study of the singular term in mixed adhesive joints. International Journal of Adhesion and Adhesives 76, 11-16.

Burchardt, B. (2011). Automotive Industry. Handbook of Adhesion Technology. L. F. M. da Silva, A. Öchsner and R. D. Adams, Springer.**:** 1186-1212.

Campilho, R. D. S. G., Banea, M. D., Neto, J. A. B. P. and da Silva, L. F. M., 2013. Modelling adhesive joints with cohesive zone models: effect of the cohesive law shape of the adhesive layer. International Journal of Adhesion and Adhesives 44, 48-56.

Campilho, R. D. S. G., Banea, M. D., Pinto, A. M. G., da Silva, L. F. M. and de Jesus, A. M. P., 2011. Strength prediction of single- and double-lap joints by standard and extended finite element modelling. International Journal of Adhesion and Adhesives 31(5), 363-372.

Campilho, R. D. S. G., de Moura, M. F. S. F. and Domingues, J. J. M. S., 2009. Numerical prediction on the tensile residual strength of repaired CFRP under different geometric changes. International Journal of Adhesion and Adhesives 29(2), 195-205.

Carvalho, U. T. F. and Campilho, R. D. S. G., 2016. Application of the direct method for cohesive law estimation applied to the strength prediction of double-lap joints. Theoretical and Applied Fracture Mechanics 85, Part A, 140-148.

da Silva, L. F. M. and Adams, R. D., 2007. Adhesive joints at high and low temperatures using similar and dissimilar adherends and dual adhesives. International Journal of Adhesion and Adhesives 27(3), 216-226.

da Silva, L. F. M., de Magalhães, A. G. and de Moura, M. F. S. F. (2007). Juntas Adesivas Estruturais. Porto, Publindustria.

da Silva, L. F. M. and Lopes, M. J. C. Q., 2009. Joint strength optimization by the mixed-adhesive technique. International Journal of Adhesion and Adhesives 29(5), 509-514.

da Silva, L. F. M., Öchsner, A. and Adams, R. D., Eds. (2011). Handbook of adhesion technology. Heidelberg, Springer.

Davies, P. (2011). Marine Industry. Handbook of Adhesion Technology. L. F. M. da Silva, A. Öchsner and R. D. Adams, Springer.**:** 1238-1262.

Désagulier, C. (2011). Aerospace Industry. Handbook of Adhesion Technology. L. F. M. da Silva, A. Öchsner and R. D. Adams, Springer**:** 1150-1184.

Dimitri, R., Trullo, M., De Lorenzis, L. and Zavarise, G., 2015. Coupled cohesive zone models for mixed-mode fracture: A comparative study. Engineering Fracture Mechanics 148, 145-179.

Hart-Smith, L. J. (2011). Adhesively Bonded Joints in Aircraft Structures. Handbook of Adhesion Technology. L. F. M. da Silva, A. Öchsner and R. D. Adams, Springer.**:** 1104-1147.

Hartung, I. and Boehm, S. (2011). Civil Construction. Handbook of Adhesion Technology. L. F. M. da Silva, A. Öchsner and R. D. Adams, Springer**:** 1264-1288.

Jairaja, R. and Naik, G. N., 2019. Single and dual adhesive bond strength analysis of single lap joint between dissimilar adherends. International Journal of Adhesion and Adhesives 92, 142-153.

Jung, S.-B. and Kim, J.-W. (2011). Electrical Industry. Handbook of Adhesion Technology. L. F. M. da Silva, A. Öchsner and R. D. Adams, Springer**:** 1290-1313.

Leitão, A. C. C., Campilho, R. D. S. G. and Moura, D. C., 2016. Shear Characterization of Adhesive Layers by Advanced Optical Techniques. Experimental Mechanics 56, 493-506.

Luo, H., Yan, Y., Zhang, T. and Liang, Z., 2016. Progressive failure and experimental study of adhesively bonded composite single-lap joints subjected to axial tensile loads. Journal of Adhesion Science and Technology 30(8), 894-914.

Martín-Martínez, J. M. (2011). Shoe Industry. Handbook of Adhesion Technology. L. F. M. da Silva, A. Öchsner and R. D. Adams, Springer**:** 1316-1347.

Öz, Ö. and Özer, H., 2017. An experimental investigation on the failure loads of the mono and bi-adhesive joints. Journal of Adhesion Science and Technology 31(19-20), 2251-2270.

Pandey, P. C. and Narasimhan, S., 2001. Three-dimensional nonlinear analysis of adhesively bonded lap joints considering viscoplasticity in adhesives. Computers & Structures 79(7), 769-783.

Petrie, E. M. (2000). Handbook of Adhesives and Sealants. United States of America, R. R. Donnelley & Sons Company.

Rocha, R. J. B. and Campilho, R. D. S. G., 2018. Evaluation of different modelling conditions in the cohesive zone analysis of single-lap bonded joints. The Journal of Adhesion 94(7), 562-582.

Sane, A. U., Padole, P. M., Manjunatha, C. M., Uddanwadiker, R. V. and Jhunjhunwala, P., 2018. Mixed mode cohesive zone modelling and analysis of adhesively bonded composite T-joint under pull-out load. Journal of the Brazilian Society of Mechanical Sciences and Engineering 40(3), 167.

Silva, J. O. S., Campilho, R. D. S. G. and Rocha, R. J. B., 2018. Crack growth analysis of adhesively-bonded stepped joints in aluminium structures. Journal of the Brazilian Society of Mechanical Sciences and Engineering 40(11), 540.

Suzuki, Y. (2011). Railway Industry. Handbook of Adhesion Technology. L. F. M. da Silva, A. Öchsner and R. D. Adams, Springer**:** 1214-1236.